SCIENCE CHINA
Information Sciences

• RESEARCH PAPER •

October 2020, Vol. 63 202402:1–202402:8
https://doi.org/10.1007/s11432-019-2778-8

Reconfigurable vertical field-effect transistor based on graphene/$MoTe_2$/graphite heterostructure

Cong WANG†, Chen PAN†, Shi-Jun LIANG, Bin CHENG* & Feng MIAO*

National Laboratory of Solid State Microstructures, School of Physics, Collaborative Innovation Center of Advanced Microstructures, Nanjing University, Nanjing 210093, *China*

Received 3 November 2019/Revised 25 December 2019/Accepted 21 January 2020/Published online 3 September 2020

Abstract Reconfigurable field-effect transistors have attracted enormous attention over the past decades because of their potential in implementing logic and analog circuit functions with fewer resources of transistors compared with complementary metal-oxide-semiconductor transistors. However, the miniaturization of traditional reconfigurable transistors is still a challenge owing to their inherent planar multi-gate structure. Herein, we fabricated a dual-gate vertical transistor based on graphene/$MoTe_2$/graphite van der Waals heterostructure and demonstrated a switchable n-type, V-shape ambipolar and p-type field-effect characteristics by varying the voltages of the top gate and drain electrodes. According to the band diagram analysis, we reveal that the reconfiguring ability of the field-effect characteristics stems from the asymmetric injection efficiency of the carriers through the gate-tunable barriers at the interfaces. Our results offer a potential approach to achieve device miniaturization of reconfigurable transistors.

Keywords reconfigurable field-effect transistor, vertical transistor, graphene/$MoTe_2$, van der Waals heterostructure, ambipolar transistor, dual-gate transistor

Citation Wang C, Pan C, Liang S-J, et al. Reconfigurable vertical field-effect transistor based on graphene/$MoTe_2$/graphite heterostructure. Sci China Inf Sci, 2020, 63(10): 202402, https://doi.org/10.1007/s11432-019-2778-8

1 Introduction

Traditional n and p-type field-effect transistors (FET) are building blocks for integrated digital and analog circuits. However, the specific field effect characteristic of a traditional FET device cannot be changed owing to using the chemical doping approach. These types of FETs are facing challenge in meeting the increasing demands for massive data processing. To overcome these challenges, reconfigurable FETs (RFETs) based on materials with ambipolar field-effect characteristics [1–13] that possess different operation modes and multiple functions, [14–24] were proposed as a promising solution to build multifunctional circuits with fewer compounds [16, 25–28]. Previously reported RFETs are based on a dual-gate planar structure [29–31]. The footprint of the RFETs has no advantage over that of the conventional FETs, which is undesirable to the high-density integration of RFETs. Fortunately, the vertical transistor [32–49] provides an alternative approach to realize RFETs with a compact structure, which is promising in the high-density integration of RFETs. In this article, we demonstrate a new reconfigurable vertical field-effect transistor (RVFET) based on graphene/$MoTe_2$/graphite vertical van der Waals (vdW) heterostructures. Our device exhibits reconfigurable features among n-type, p-type, and V-shape ambipolar field-effect characteristics by reconfiguring the gate and drain-source bias voltages. Furthermore,

* Corresponding author (email: bincheng@nju.edu.cn, miao@nju.edu.cn)
† Wang C and Pan C have the same contribution to this work.

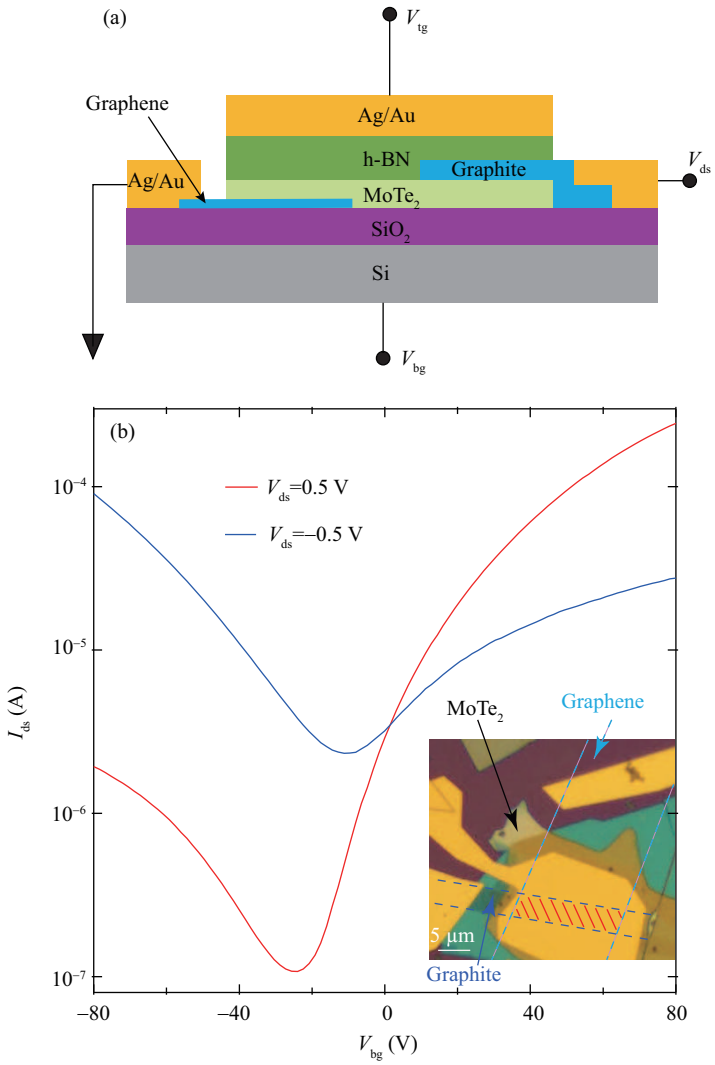

Figure 1 (Color online) Device structure and bottom gate field-effect characteristics of the RVFET. (a) Schematic of the RVFET based on graphene/$MoTe_2$/graphite vertical van der Waals heterostructure. (b) Field-effect of drain-source current versus bottom gate voltage under different V_{ds} biases. The inset shows the optical micrograph of the RVFET.

we have employed the band diagrams to illustrate that the asymmetrically gate-tunable Schottky barriers at the interfaces determine the working mechanism of the RVFET. Our work opens an opportunity to achieve high-density integrated reconfigurable circuit applications.

2 Results and discussion

As shown schematically in Figure 1(a), we have fabricated the RVFET device by employing vdW heterostructures comprised of monolayer graphene, graphite (∼3 nm), $MoTe_2$ (∼24 nm), and h-BN (∼20 nm). All materials were mechanically exfoliated on SiO_2/Si substrate and then stacked by the polyvinyl alcohol (PVA) transfer method. Specifically, we use $MoTe_2$ as the channel material, graphene as the bottom electrode (source terminal), graphite as the top electrode (drain terminal), Ag/Au metal as the top gate, p-Si as the bottom gate, h-BN and 300 nm SiO_2 as their insulating layers. The channel length of the RVFET is defined by the thickness of $MoTe_2$ flake (see Figure S1). To ensure the high quality of the prepared materials, the Raman spectra of all the materials mentioned above were characterized before the transfer process (see Figure S2) [50, 51]. The standard electron beam lithography and electron beam evaporation processes were carried out to fabricate Ag (5 nm)/Au (40 nm) metal electrodes to form ohmic

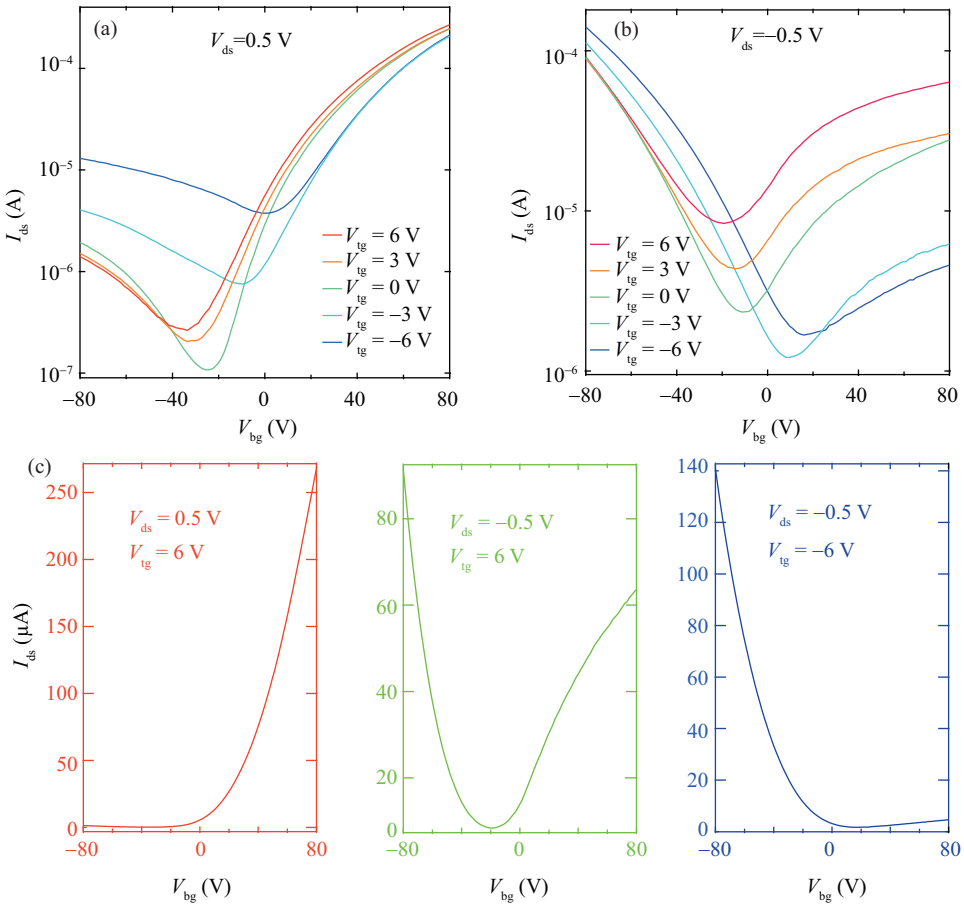

Figure 2 (Color online) Reconfigurable electrical performance of RVFET. (a), (b) Field-effect transfer curves at ±0.5 V $V_{\rm ds}$ and different $V_{\rm tg}$ varies between −6 V and 6 V. (c) The typical n-type, V-shape, and p-type transfer characteristic curves from the same RVFET device by reconfiguring the bias voltages of $V_{\rm ds}$ and $V_{\rm tg}$.

contact with graphene and graphite. The device was then annealed at 280°C in Ar ambience for 2 h to remove resist residue and improve the contact between the metal and 2D material. A representative optical microscope image of RVFET is shown in the inset of Figure 1(b).

To study the reconfigurable field-effect characteristics of RVFET in detail, we first examined the drain current ($I_{\rm ds}$) of the RVFET by sweeping the back-gate voltage ($V_{\rm bg}$) with the top gate floated. The V-shape transfer characteristic curves exhibited in Figure 1(b) illustrate the ambipolar field-effect characteristics with both positive (red curve) and negative (blue curve) drain-to-source voltage ($V_{\rm ds}$). The n-branch of the field-effect current in the region of $V_{\rm bg} < V_{\rm Imin}$ ($V_{\rm Imin}$, the gate voltage when $I_{\rm ds}$ is minimized) is dominated by the electron injection from the graphene electrode at positive $V_{\rm ds}$ (red curve) and graphite electrodes at negative $V_{\rm ds}$ (blue curve). On the other hand, the p-branch field-effect current with $V_{\rm bg} > V_{\rm Imin}$ is determined by hole injection, and the carrier injection source is different from the n-branch. Note that the p-branch current under the negative $V_{\rm ds}$ is much larger than that under the positive $V_{\rm ds}$, while the n-branch current under the negative $V_{\rm ds}$ is smaller than that under the positive $V_{\rm ds}$. This result suggests that the carrier injection efficiency at the graphene/$MoTe_2$ interface is higher than that at the graphite/$MoTe_2$ interface. This phenomenon is because the Fermi level in the graphene can be adjusted while the Fermi level in the graphite is fixed. Furthermore, the field-effect of $I_{\rm ds}$ versus top gate $V_{\rm tg}$ was also measured, with the results shown in Figure S3, which demonstrates field effect characteristics similar to the V-shape one. All of the above results indicate that RVFETs can exhibit reconfigurable electrical characteristics under the different configurations of $V_{\rm ds}$, $V_{\rm tg}$, and $V_{\rm bg}$.

The demonstrated field-effect characteristics of both top and bottom gates allows us to further explore the reconfigurable field-effect characteristics of the RVFET by tuning $V_{\rm ds}$, $V_{\rm bg}$, and $V_{\rm tg}$ voltages. As

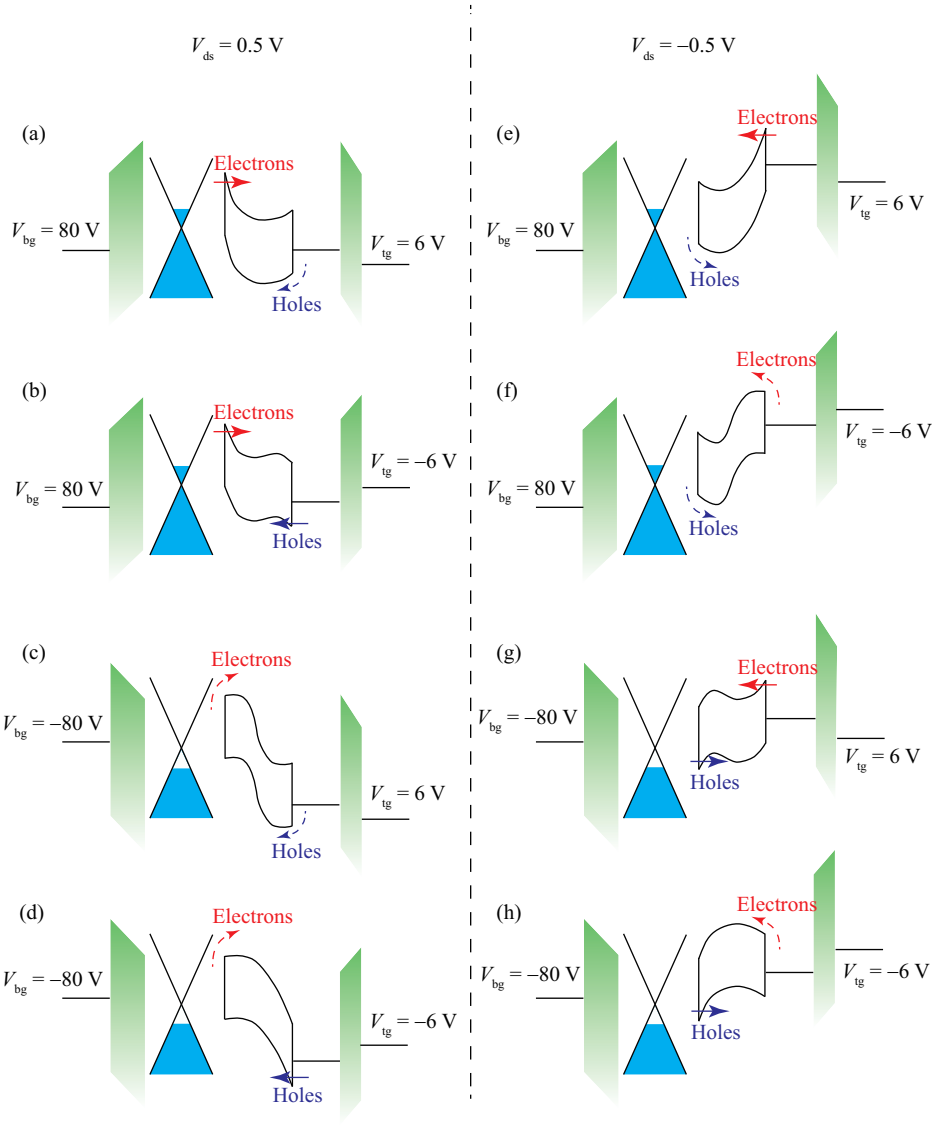

Figure 3 (Color online) Band diagrams of RVFET corresponding to eight carrier transport regimes (a)–(h) that are the different combinations of the V_{bg} (80 or −80 V), V_{tg} (6 or −6 V), and V_{ds} (0.5 or −0.5 V). Thick solid and thin dashed lines indicate majority and minority injection of the charge carriers, respectively.

shown in the Figure 2(a), when V_{ds} is positive and V_{tg} varies from 6 to −6 V, the n-branch field-effect curves almost overlap, while the p-branch current is enhanced as the V_{tg} decreases, indicating that the hole injection from the drain electrode could be modulated by changing V_{tg}. Meanwhile, inverse gate-dependent behaviors are observed under the negative V_{ds}, as shown in Figure 2(b). The field effect characteristics by sweeping V_{tg} and output characteristics curves of RVFET are also given in Figures S4 and S5, respectively. Notably, by reconfiguring V_{ds} and V_{tg}, we have successfully demonstrated the n-type, V-shape ambipolar and p-type field-effect characteristics in the same device (see Figure 2(c)). Our RVFET technology has an obvious advantage over the prior work reporting different field-effect characteristics by varying thickness [52], as we achieved reconfigurable field-effect characteristics by only tuning the polarity of the voltage. We also compare the RVFET with different dual-gate reconfigurable FET devices, as shown in Table S1.

To understand the working mechanism of the RVFET, we drew a group of band diagrams in the graphene/$MoTe_2$/graphite vertical vdW heterostructure. Specifically, we divided all configurations of the bottom gate, top gate, and drain-source bias voltages into eight carrier transport regimes that are different combinations of the V_{bg} (80 or −80 V), V_{tg} (6 or −6 V), and V_{ds} (0.5 or −0.5 V) corresponding

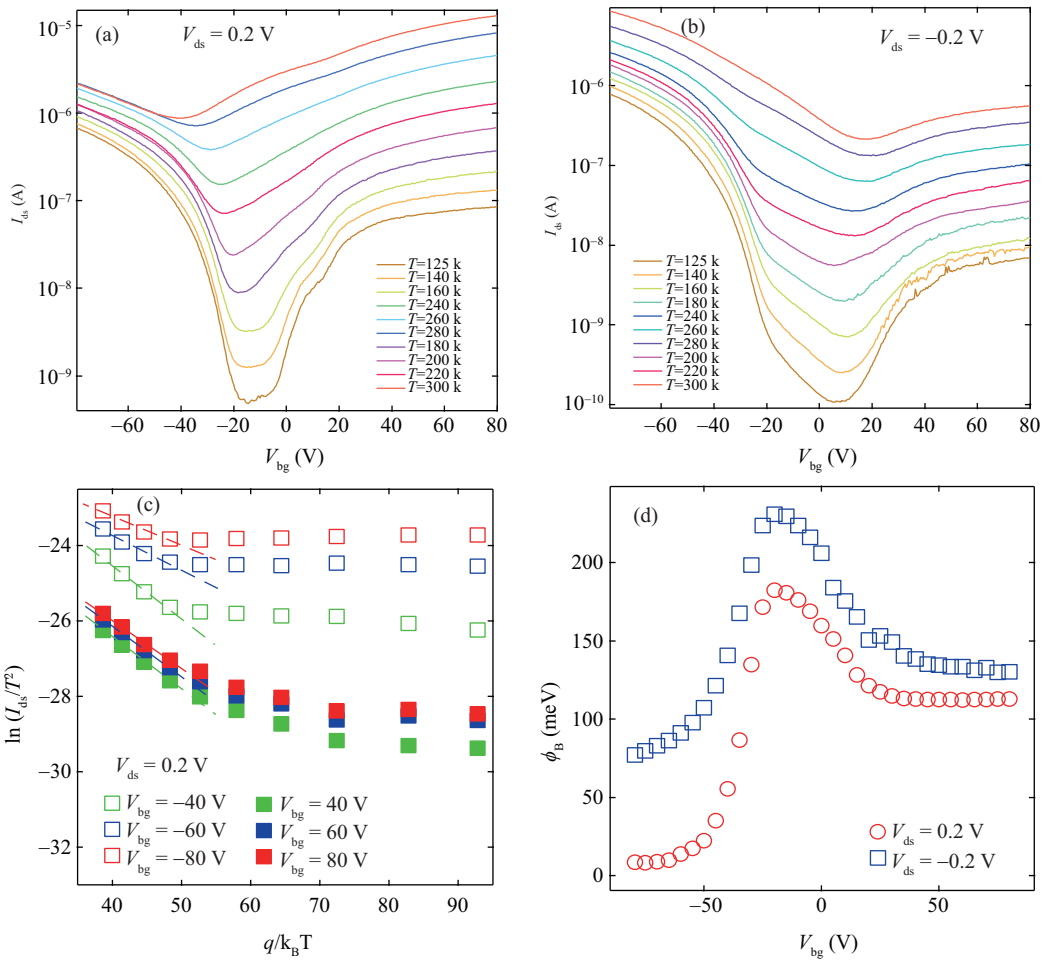

Figure 4 (Color online) Temperature-dependent charge transport of RVFET. Field-effect transfer characteristics by sweeping V_{bg} at different temperatures ranging from 125 to 300 K with $V_{ds} = 0.2$ V in (a) and $V_{ds} = -0.2$ V in (b). (c) Arrhenius plot at $V_{ds} = 0.2$ V with V_{bg} varying from −80 to −40 V (p-branch) and 40 to 80 V (n-branch). (d) Variation of effective barrier height extracted from the slope of the fitted lines in (c). The top gate was floated in this test.

to the band diagrams (Figures 3(a)–(h)). The direction of the carrier flow is determined by the bias polarity of V_{ds}. In the regimes with positive V_{ds} (Figures 3(a)–(d)), the electrons (holes) traverse $MoTe_2$ from graphene (graphite) electrode to the graphite (graphene) electrode, while carrier transport direction in those regimes with negative V_{ds} is inversed, as shown in Figures 3(e)–(h). As long as the carrier flow direction is determined, energy band bending modes at graphene/$MoTe_2$ and $MoTe_2$/graphite interfaces that are controlled by V_{bg} and V_{tg} determine the ability for the carriers to pass the barrier and further affect the current state (on or off) of the transistor.

We specifically focused on a regime to elucidate the mechanism in detail (as shown in the Figure 3(a)), where V_{ds}, V_{bg}, and V_{tg} are positive. The valence and conduction band of $MoTe_2$ bend downward, and the raised Fermi level of graphene results in the thinned and lowered Schottky barrier at the graphene/$MoTe_2$ interface that facilitates the electron injection as indicated by the solid line arrows. On the other hand, according to the increased Schottky barrier, the hole injection is blocked at the $MoTe_2$/graphite interface, as indicated by the dashed line arrows. Therefore, the transport property of the device in regime a is dominated by electrons, which agrees well with the n-branch of the red transfer curve in the Figure 2(a). If we tune V_{bg} to be negative while keeping V_{ds} and V_{tg} unchanged, as shown in the Figure 3(c), the Fermi level of the graphene is lowered, and the energy band of $MoTe_2$ bends upward at the graphene/$MoTe_2$ interface, resulting in an increased Schottky barrier and then blocking the electron injection. Considering that hole injection is blocked at the $MoTe_2$/graphite interface owing to the same reason as mentioned above, we could obtain a low current level corresponding to the p-branch of the red curve in the Figure 2(a).

Therefore, the n-type field-effect characteristics as shown in the left panel of the Figure 2(c) could be explained by Figure 3(a) and (c). Similarly, the n and p-branch of the V-shape ambipolar field-effect characteristic shown in the middle panel of the Figure 2(c) could be explained using the band diagram in Figure 3(e) and (g), respectively. Meanwhile, the p-type field-effect characteristic shown in the right panel of the Figure 2(c) corresponds to the carrier injection indicated in Figure 3(f) and (h), in which the hole injection dominates the on-state current.

Based on the analysis above, we believe that the tunable Schottky barriers are responsible for the reconfigurable behaviors of RVFETs. This conclusion is further justified using the experimental results of temperature-dependent charge transport (see Figure 4). Note that graphene has a smaller electronic density of states than graphite, and the field-effect in the graphene is more profound within the same range of the gate voltage compared to the graphite. Therefore, the variation of the Schottky barrier height at the interface of graphene/$MoTe_2$ is larger than that of $MoTe_2$/graphite. In other words, it is the asymmetric tunability of the carrier injection at graphene/$MoTe_2$ and $MoTe_2$/graphite interfaces that leads to the reconfigurable field-effect characteristics of the RVFET.

3 Conclusion

We have successfully fabricated the RVFET based on the graphene/$MoTe_2$/graphite vdW heterojunction with a vertical dual-gate structure. By varying the drain-to-source bias and the top gate voltage, we demonstrated that the RVFET could exhibit three distinct types of field-effect characteristics, i.e., n-type, V-shape ambipolar, and p-type field-effect characteristics. Moreover, we used the band diagrams to reveal that gate-tunable asymmetric Schottky barriers in the graphene/$MoTe_2$/graphite vdW heterojunction could account for the reconfigurable field-effect characteristics of the RVFET. Our work offers new insight in designing a reconfigurable FET to address the challenge of device miniaturization.

Acknowledgements This work was supported in part by National Key Basic Research Program of China (Grant No. 2015CB921600), National Natural Science Foundation of China (Grant Nos. 61974176, 61574076, 61921005), Natural Science Foundation of Jiangsu Province (Grant Nos. BK20180330, BK20150055), and Fundamental Research Funds for the Central Universities (Grant Nos. 020414380122, 020414380084).

Supporting information Figures S1–S5 and Table S1. The supporting information is available online at info.scichina.com and link.springer.com. The supporting materials are published as submitted, without typesetting or editing. The responsibility for scientific accuracy and content remains entirely with the authors.

References

1 Yang X B, Liu G X, Balandin A A, et al. Triple-mode single-transistor graphene amplifier and its applications. ACS Nano, 2010, 4: 5532–5538
2 Moon J S, Curtis D, Zehnder D, et al. Low-phase-noise graphene FETs in ambipolar RF applications. IEEE Electron Dev Lett, 2011, 32: 270–272
3 Jariwala D, Sangwan V K, Seo J W T, et al. Large-area, low-voltage, antiambipolar heterojunctions from solution-processed semiconductors. Nano Lett, 2015, 15: 416–421
4 Wang Z X, Ding L, Pei T, et al. Large signal operation of small band-gap carbon nanotube-based ambipolar transistor: a high-performance frequency doubler. Nano Lett, 2010, 10: 3648–3655
5 Wang H, Hsu A, Wu J, et al. Graphene-based ambipolar RF mixers. IEEE Electron Dev Lett, 2010, 31: 906–908
6 Han S J, Garcia A V, Oida S, et al. Graphene radio frequency receiver integrated circuit. Nat Commun, 2014, 5: 3086
7 Wang H, Nezich D, Kong J, et al. Graphene frequency multipliers. IEEE Electron Dev Lett, 2009, 30: 547–549
8 Guerriero E, Polloni L, Rizzi L G, et al. Graphene audio voltage amplifier. Small, 2012, 8: 357–361
9 Yang X B, Liu G X, Rostami M, et al. Graphene ambipolar multiplier phase detector. IEEE Electron Dev Lett, 2011, 32: 1328–1330
10 Zhu W N, Yogeesh M N, Yang S X, et al. Flexible black phosphorus ambipolar transistors, circuits and AM demodulator. Nano Lett, 2015, 15: 1883–1890
11 Lee S, Lee K, Liu C H, et al. Flexible and transparent all-graphene circuits for quaternary digital modulations. Nat Commun, 2012, 3: 1018

12 Palacios T, Hsu A, Wang H. Applications of graphene devices in RF communications. IEEE Commun Mag, 2010, 48: 122–128

13 Wang Z X, Zhang Z Y, Xu H L, et al. A high-performance top-gate graphene field-effect transistor based frequency doubler. Appl Phys Lett, 2010, 96: 173104

14 de Marchi M, Sacchetto D, Frache S, et al. Polarity control in double-gate, gate-all-around vertically stacked silicon nanowire fets. In: Proceedings of International Electron Devices Meeting, 2012

15 Yoo H, Smits E C P, van Breemen A J, et al. Asymmetric split-gate ambipolar transistor and its circuit application to complementary inverter. Adv Mater Technol, 2016, 1: 1600044

16 Zhang J, de Marchi M, Sacchetto D, et al. Polarity-controllable silicon nanowire transistors with dual threshold voltages. IEEE Trans Electron Dev, 2014, 61: 3654–3660

17 Heinzig A, Mikolajick T, Trommer J, et al. Dually active silicon nanowire transistors and circuits with equal electron and hole transport. Nano Lett, 2013, 13: 4176–4181

18 Heinzig A, Slesazeck S, Kreupl F, et al. Reconfigurable silicon nanowire transistors. Nano Lett, 2012, 12: 119–124

19 Zhao Y J, Candebat D, Delker C, et al. Understanding the impact of Schottky barriers on the performance of narrow bandgap nanowire field effect transistors. Nano Lett, 2012, 12: 5331–5336

20 Resta G V, Balaji Y, Lin D, et al. Doping-free complementary logic gates enabled by two-dimensional polarity-controllable transistors. ACS Nano, 2018, 12: 7039–7047

21 Pang C, Thakuria N, Gupta S K, et al. First demonstration of Wse_2 based CMOS-SRAM. In: Proceedings of International Electron Devices Meeting (IEDM), 2018

22 Pang C S, Chen Z H. First demonstration of WSe_2 CMOS inverter with modulable noise margin by electrostatic doping. In: Proceedings of the 76th Device Research Conference (DRC), 2018

23 Liu Y, Zhang G, Zhou H L, et al. Ambipolar barristors for reconfigurable logic circuits. Nano Lett, 2017, 17: 1448–1454

24 Larentis S, Fallahazad B, Movva H C P, et al. Reconfigurable complementary monolayer $MoTe_2$ field-effect transistors for integrated circuits. ACS Nano, 2017, 11: 4832–4839

25 Mongillo M, Spathis P, Katsaros G, et al. Multifunctional devices and logic gates with undoped silicon nanowires. Nano Lett, 2012, 12: 3074–3079

26 Trommer J, Heinzig A, Slesazeck S, et al. Elementary aspects for circuit implementation of reconfigurable nanowire transistors. IEEE Electron Dev Lett, 2014, 35: 141–143

27 Gaillardon P E, Tang X F, Kim G, et al. A novel FPGA architecture based on ultrafine grain reconfigurable logic cells. IEEE Trans VLSI Syst, 2015, 23: 2187–2197

28 Ben-Jamaa M H, Mohanram K, de Micheli G. An efficient gate library for ambipolar CNTFET logic. IEEE Trans Comput-Aided Des Integr Circ Syst, 2011, 30: 242–255

29 Mikolajick T, Heinzig A, Trommer J, et al. The RFET-a reconfigurable nanowire transistor and its application to novel electronic circuits and systems. Semicond Sci Technol, 2017, 32: 043001

30 Trommer J, Heinzig A, Heinrich A, et al. Material prospects of reconfigurable transistor (RFETs) — from silicon to germanium nanowires. MRS Proc, 2014, 1659: 225–230

31 Weber W M, Heinzig A, Trommer J, et al. Reconfigurable nanowire electronics — a review. Solid-State Electron, 2014, 102: 12–24

32 Georgiou T, Jalil R, Belle B D, et al. Vertical field-effect transistor based on graphene-WS_2 heterostructures for flexible and transparent electronics. Nat Nanotech, 2013, 8: 100–103

33 Liu Y, Weiss N O, Duan X D, et al. Van der Waals heterostructures and devices. Nat Rev Mater, 2016, 1: 16042

34 Kang J, Jariwala D, Ryder C R, et al. Probing out-of-plane charge transport in black phosphorus with graphene-contacted vertical field-effect transistors. Nano Lett, 2016, 16: 2580–2585

35 Yu W J, Li Z, Zhou H L, et al. Vertically stacked multi-heterostructures of layered materials for logic transistors and complementary inverters. Nat Mater, 2013, 12: 246–252

36 Choi Y, Kang J, Jariwala D, et al. Low-voltage complementary electronics from ion-gel-gated vertical van der Waals heterostructures. Adv Mater, 2016, 28: 3742–3748

37 Moriya R, Yamaguchi T, Inoue Y, et al. Large current modulation in exfoliated-graphene/MoS_2/metal vertical heterostructures. Appl Phys Lett, 2014, 105: 083119

38 Moriya R, Yamaguchi T, Inoue Y, et al. Influence of the density of states of graphene on the transport properties of graphene/MoS_2/metal vertical field-effect transistors. Appl Phys Lett, 2015, 106: 223103

39 Shim J, Kim H S, Shim Y S, et al. Extremely large gate modulation in vertical graphene/WSe_2 heterojunction barristor based on a novel transport mechanism. Adv Mater, 2016, 28: 5293–5299

40 Sata Y, Moriya R, Morikawa S, et al. Electric field modulation of Schottky barrier height in graphene/$MoSe_2$ van der Waals heterointerface. Appl Phys Lett, 2015, 107: 023109

41 Lin Y F, Li W W, Li S L, et al. Barrier inhomogeneities at vertically stacked graphene-based heterostructures.

Nanoscale, 2014, 6: 795–799
42 Liu Y, Zhou H L, Cheng R, et al. Highly flexible electronics from scalable vertical thin film transistors. Nano Lett, 2014, 14: 1413–1418
43 Parui S, Pietrobon L, Ciudad D, et al. Gate-controlled energy barrier at a graphene/molecular semiconductor junction. Adv Funct Mater, 2015, 25: 2972–2979
44 Liu J Y, Zhou K, Liu J, et al. Organic-single-crystal vertical field-effect transistors and phototransistors. Adv Mater, 2018, 30: 1803655
45 Liu Y, Guo J, Zhu E B, et al. Maximizing the current output in self-aligned graphene-InAs-metal vertical transistors. ACS Nano, 2019, 13: 847–854
46 Liu J Y, Qin Z S, Gao H K, et al. Vertical organic field-effect transistors. Adv Funct Mater, 2019, 29: 1808453
47 Pan C, Fu Y J, Wang J X, et al. Analog circuit applications based on ambipolar graphene/$MoTe_2$ vertical transistors. Adv Electron Mater, 2018, 4: 1700662
48 Liang S J, Cheng B, Cui X, et al. Van der Waals heterostructures for high-performance device applications: challenges and opportunities. Adv Mater, 2019, 306: 1903800
49 Hui F. Chemical vapor deposition of hexagonal boron nitride and its use in electronic devices. 2018. ArXiv:1905.06938
50 Fathipour S, Ma N, Hwang W S, et al. Exfoliated multilayer $MoTe_2$ field-effect transistors. Appl Phys Lett, 2014, 105: 192101
51 Ferrari A C, Meyer J C, Scardaci V, et al. Raman spectrum of graphene and graphene layers. Phys Rev Lett, 2006, 97: 187401
52 Zhou C J, Zhao Y D, Raju S, et al. Carrier type control of WSe_2 field-effect transistors by thickness modulation and MoO_3 layer doping. Adv Funct Mater, 2016, 26: 4223–4230